

Anomalous thermal effect in ZrTe₅ observed via photothermal measurements

M. Tsuneto, Q. Li

To be published in "Physical Review Applied"

March 2024

Condensed Matter Physics and Materials Science Department
Brookhaven National Laboratory

U.S. Department of Energy
USDOE Office of Science (SC), Basic Energy Sciences (BES)

Notice: This manuscript has been authored by employees of Brookhaven Science Associates, LLC under Contract No. DE-SC0012704 with the U.S. Department of Energy. The publisher by accepting the manuscript for publication acknowledges that the United States Government retains a non-exclusive, paid-up, irrevocable, world-wide license to publish or reproduce the published form of this manuscript, or allow others to do so, for United States Government purposes.

DISCLAIMER

This report was prepared as an account of work sponsored by an agency of the United States Government. Neither the United States Government nor any agency thereof, nor any of their employees, nor any of their contractors, subcontractors, or their employees, makes any warranty, express or implied, or assumes any legal liability or responsibility for the accuracy, completeness, or any third party's use or the results of such use of any information, apparatus, product, or process disclosed, or represents that its use would not infringe privately owned rights. Reference herein to any specific commercial product, process, or service by trade name, trademark, manufacturer, or otherwise, does not necessarily constitute or imply its endorsement, recommendation, or favoring by the United States Government or any agency thereof or its contractors or subcontractors. The views and opinions of authors expressed herein do not necessarily state or reflect those of the United States Government or any agency thereof.

Anomalous thermal effect in ZrTe₅ observed via photothermal measurements

Makoto Tsuneto¹, Ran Jing^{1,2}, Xinzhong Chen¹, Sahal Kaushik^{1,3}, Juntao Yao^{2,5}, Dmitri E. Kharzeev^{1,6,7}, Xu Du¹, Qiang Li^{1,2}, Mengkun Liu^{1,4*}

¹*Department of Physics and Astronomy, Stony Brook University, Stony Brook, New York 11794, USA*

²*Condensed Matter Physics and Materials Science Department, Brookhaven National Lab, Upton, New York 11973, USA.*

³*Nordita, Stockholm University and KTH Royal Institute of Technology, SE-106 91 Stockholm, Sweden.*

⁴*National Synchrotron Light Source II, Brookhaven National Laboratory, Upton, NY, USA*

⁵*Department of Materials Science and Chemical Engineering, Stony Brook University, Stony Brook, New York 11794-3800, USA*

⁶*Department of Physics, Brook Haven National Laboratory, Upton, New York 11973-5000, USA*

⁷*RIKEN-BNL Research Center, Brook Haven National Laboratory, Upton, New York 11973-5000, USA*

*Corresponding authors: mengkun.liu@stonybrook.edu,

Abstract

In this study, we explore the magneto-thermoelectric power (MTP) of ZrTe₅, a canonical Dirac semimetal, through a novel photothermal technique. Unlike conventional thermoelectric studies that rely on on-chip heaters and are limited by fabrication processes, especially for stress-sensitive materials, our approach utilizes photothermal effects to induce temperature gradients. Our experiments, applying a magnetic field approximately parallel and transverse to the photocurrent detection direction, reveal that the photothermal method efficiently and reliably extracts both diagonal and off-diagonal components of the thermoelectric coefficient of ZrTe₅. We observe that the longitudinal MTP reproduces features previously reported in thermal transport studies, while the photoinduced transverse MTP confirms the anomalous Nernst effect. This photothermal measurement technique opens new avenues for investigating transport properties in a wide range of quantum materials, both in 3D and 2D systems.

I. INTRODUCTION

In three-dimensional topological semimetals such as Dirac semimetals (DSMs) [1,2] and Weyl semimetals (WSMs) [3,4], electrons near the conduction-valence band crossing (Dirac point) behave as Dirac or Weyl fermions which have left or right handedness, so-called ‘*chirality*’ $\chi = \pm 1$ [1,3] ($\chi = \vec{p} \cdot \vec{\sigma}$ for massless particles, where \vec{p} is the momentum vector and $\vec{\sigma} = (\sigma_x, \sigma_y)$ is the Pauli matrix). A particularly interesting phenomenon of these fermions is called chiral anomaly, where the symmetry of the left and right chirality is violated. The anomaly contributes to the chiral magnetic effect (CME) that a chiral charge current can be induced by a non-trivial arrangement of external fields, specifically parallel electric and magnetic fields [5,6]. CME underpins a wide palette of new and exciting phenomena, such as near dissipation-less charge transport [7], negative magnetoresistance (MR), and chiral magnetic photocurrent [8].

The CME has a unique magnetic field dependence. In the presence of coupling between chiral fermions and electromagnetic field, gauge symmetry requires that chiral charge density, that is, the difference between the charge density of left- and right-handedness ($\rho_5 \equiv \rho_R - \rho_L$), changes with an external electric field parallel with the magnetic field [9]. With a finite static magnetic field, the conductivity has an additional contribution called chiral magnetic conductivity [5,6]:

$$\Delta\sigma_{CME}^{zz} \propto B^2. \quad (1)$$

Here, the index zz denotes the longitudinal conductivity caused by the parallel electric and magnetic field (along the direction of fields). In other words, CME manifests itself as an extra conductivity quadratic in the magnetic field, that is, negative MR. This phenomenon was first measured in ZrTe₅[10] and later in Na₃Bi[11], Cd₃As₂ [12,13], TaAs[14], NbAs [15], TaP[16], etc. According to the well-known Mott relation [17], thermoelectric coefficients also acquire a characteristic field dependence at low fields. In such situations, the Mott formula relates $\Delta\sigma_{CME}^{zz}$ and the (longitudinal) thermopower S_{zz} . In the leading order, S_{zz} depends on B^2 as follows[18]:

$$\frac{S_{zz}(B)}{S_{zz}(0)} = \left(1 - \frac{B^2}{B_0^2}\right) \left(1 + \frac{B^2}{B_0^2}\right)^{-1}. \quad (2)$$

For instance, DC transport results of Cd₃As₂ with an on-chip heater are well-fitted by Eq. (1) and (2) [19]. Moreover, a recent study of ZrTe₅ further examined those anomalous behaviors in detail, showing that they are highly sensitive to the alignment of the magnetic field with the a -axis [20].

ZrTe₅, as a 3D Dirac semimetal, has been shown to be a good platform for exploring many macroscopic quantum phenomena. Depending on the sample quality, ZrTe₅ experiences a

Lifshitz transition at varied temperatures, where the hole pocket at high temperature switches to electron pocket at low temperature [21]. In the parallel electric and magnetic field configuration, ZrTe_5 exhibits CME in the electronic and thermal transport measurement [10,19,22]. In the transverse electric and magnetic field configuration, both anomalous Hall effect [23] and anomalous Nernst effect [24] have been observed in single crystal samples. The anomalous Hall effect remains in the thin devices of ZrTe_5 [25]. In few-layer samples, integer quantum Hall effect (QHE) like behavior was reported, but the original claim of 3D QHE was challenged by more recent experiments [26,27]. More intriguingly, ZrTe_5 can enter quantum-limit at low temperatures and low magnetic fields. At temperatures below 20 K, quantum oscillations can be observed in the electronic and thermal transport of ZrTe_5 , and with only a few Teslas, the electrons are confined in the lowest Landau level and thus the system enters the quantum limit [24,28,29].

In this work, we use a focused laser beam rather than an on-device heater to induce photothermal current in ZrTe_5 . By taking advantage of the Shockly-Ramo (SR) formalism [30,31], we selectively measured the diagonal and off-diagonal components in the Seebeck coefficient. This study provides a convenient and alternative method to study thermal transport behavior, without the need for an on-device heating source. In our studies, we find that the magnetic field dependence of the diagonal and off-diagonal components of the thermoelectric coefficient reproduces nearly identical behavior with previously published results using the thermal transport method with on-device heaters.

II. METHODS

The samples studied in this work are flux-grown ZrTe_5 single crystals fixed on SiO_2/Si substrate, with fresh tape-cleaved surfaces. Four 100 nm thick gold contacts were evaporated onto the sample through a shadow mask. The electrically wired samples are measured in a Quantum Design physical property measurement system (PPMS) for traditional electrical and thermal transport characterizations. The photothermal measurement is performed in a high-vacuum optical cryostat with a magnetic field up to 7 Tesla (Opticool, Quantum Design Inc.). The sample is elongated along the a-axis. The contact configuration is displayed in the inset of Fig. 1(a). In the photothermal measurements, the a-axis of the sample can be placed approximately parallel or transverse to the magnetic field. Magnetic field-dependent DC transport measurements and photocurrent measurements can be performed with a 4-probe and 2-probe schemes, respectively. For measuring the photocurrent, we use a linearly polarized CO_2 laser ($\lambda \sim 10.6 \mu\text{m}$) with a chopper of the frequency 1 kHz. The incident power is 5 mW, and the focused beam size on the sample is tens of microns in width. The gap sizes between the two inner contacts are 20 μm to 100 μm depending on the sample. Due to the thermal gradient created by the laser, photocurrent is collected across the inner pair of electrodes and measured by a lock-in amplifier. The input

impedance of the current to voltage pre-amplifier (60Ω) is much larger than the sample resistance ($< 100 \mu\Omega$). Therefore, our photocurrent measurement directly scales with the Seebeck coefficient, and the sample resistance plays a negligible role. Noticeably, we observe no significant laser polarization dependence of the photocurrent.

The theory of photothermal current collection has been well explained by the SR formalism [30–35]. The signal can be expressed as,

$$I_{PC} = \int \mathbf{j}_{pc} \cdot \nabla \phi_{SR} d^2r \propto \int \nabla T \cdot S \cdot \nabla \phi_{SR} d^2r,$$

where \mathbf{j}_{pc} is the local photocurrent density generated by a thermal distribution ∇T multiplied by the Seebeck coefficient S and regulated by the overall resistance of the circuit. $\nabla \phi_{SR}$ is an auxiliary electric field established between the source and drain contacts assuming they are at 0 V and 1 V, respectively. In our experiments, the sample and contacts are prepared in regular square shapes, so that the auxiliary field always points straightly from the drain to the source contact. With the SR formalism, we can measure one of the components in the Seebeck coefficient matrix by selectively aligning the magnetic field and beam spot.

III. RESULTS AND DISCUSSION

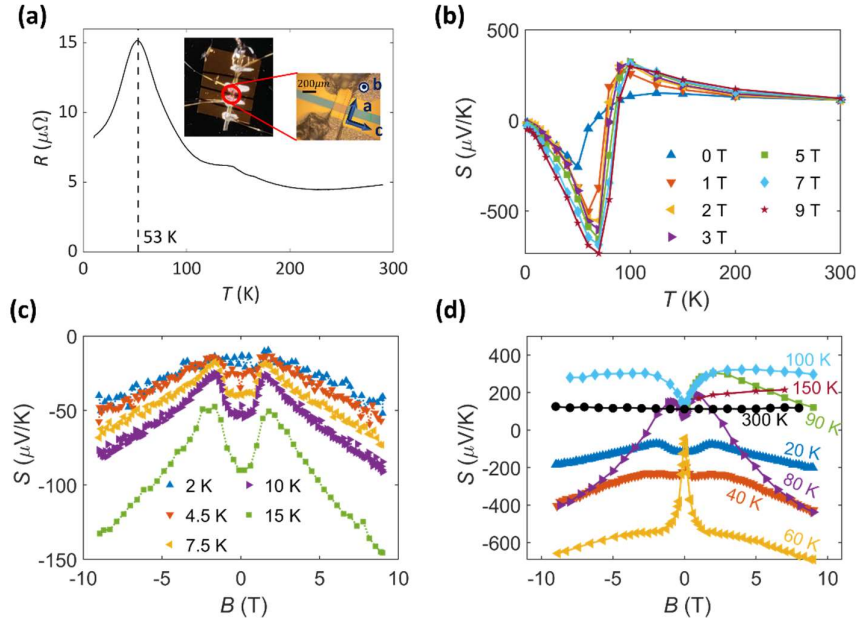


Fig. 1 Transport measurement geometry and results of ZrTe₅. (a) Result of DC transport measurements without magnetic field. Inset: Microscope images of our sample with gold electrodes (b) The temperature dependence of the longitudinal Seebeck coefficient measured by contact method. (c) and (d) The magnetic field dependence of the longitudinal Seebeck coefficient at temperatures ranging from 2 K to 300 K is measured with the magnetic field aligned along the out-of-plane direction (along b-axis of the crystal).

The DC resistance measurements are performed by the 4-probe method with 1 μA current. As seen in Fig. 1(a), the resistance peaked around $T_p \sim 53$ K due to the change in its dominant carrier type due to Lifshitz transition, consistent with previous measurements [21,36]. The measured T_p of our sample is lower than previously reported values [10,21,24,36–38], suggesting a lower defect concentration and thus good sample quality [21]. We first examined the Seebeck coefficient using thermal transport methods with the magnetic field along b-axis of the crystal. The Lifshitz transition of ZrTe_5 is manifested as a strong anomaly with or without magnetic field between 50 K and 70 K (Fig. 1(b)), consistent with previous results [21,23]. The sign-changing behavior is due to the switching of carrier type from holes above the transition to electrons below the transition. In Fig. 1(c) and 1(d), we summarized the magnetic field dependence of the Seebeck coefficient from 2 K to 300 K measured by the thermal transport method with an on-chip heater. For data below 20 K (Fig. 1(c)), we observe a clear change of field dependence at around 2 T. The negative MR at low field can be explained by the weak antilocalization in Dirac semimetals induced by magnetic fields [39–41]. The MR changes to positive at high field. The absolute value of Seebeck coefficient at a non-zero field gradually increases until 60 K (Fig. 1(d)) [21], beyond which the value quickly switches signs due to the Lifshitz transition. The transition behavior is consistent with our previous results on samples using identical preparation methods [18].

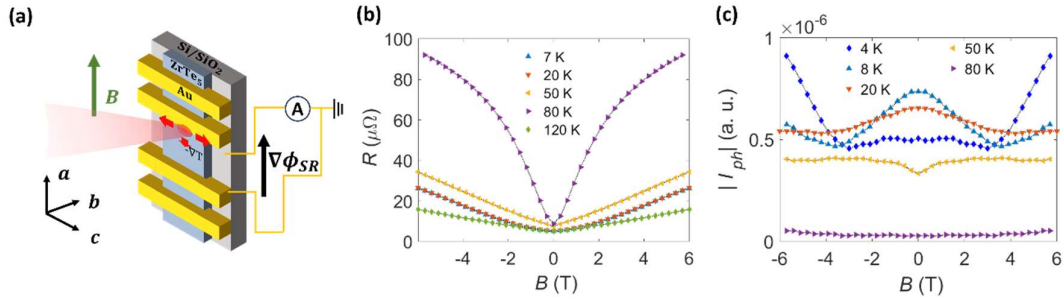


Fig. 2 Photothermal measurements of ZrTe_5 in a parallel electric and magnetic field configuration. (a) The schematics of the measurement. The magnetic field is aligned approximately along the a-axis of the crystal. The laser is focused around one of the inner contacts. The thermal distribution of the laser spot ∇T generates the local photocurrent distribution. The photocurrent is collected by the two inner contacts. (b) The magnetoresistance (MR) measured in the configuration shown in (a). The positive MR indicates that the alignment of the magnetic field is not strictly along the electric field direction. (c) The magnetothermal photocurrent measured in the configuration shown in (a). Despite the alignment of the magnetic field not being strictly in parallel electric and magnetic field configuration, the photocurrent signal shows negative field dependence at low magnetic fields.

Now, we perform photothermal current measurements to extract the magnetic field dependence of the longitudinal component of the Seebeck coefficient. The schematic of the measurement is shown in Fig. 2(a). The magnetic field is aligned approximately parallel with the a-axis of the crystal. The source and drain contacts are also aligned with the a-axis. The MR of our sample is displayed in Fig. 2(b). The result did not show negative MR due to a small misalignment of the sample a-axis with the magnetic field. As shown in Fig. 2(a), we focus the laser beam spot around one of the inner contacts. The laser generates a thermal distribution and consequently a photocurrent distribution on the sample surface. The local photocurrent distribution generated along the c and b axis of the crystal does not contribute to the acquired current because the auxiliary field defined in the SR formalism aligns from the drain to the source (along a-axis). The only contributing local term is $j_{PC,a} \propto S_{aa} \partial_a T$, and thus the collected non-local signal $I_{PC} \propto S_{aa}(B)$. In Fig. 2(c), we show the acquired magneto-thermoelectric power (MTP). We observe a negative magnetic field dependence of photothermal signal at low field and a switch to positive dependence at 3 T \sim 4 T below 20 K. This behavior is absent in our data above 50 K. Together with the positive MR, we reproduce identical features of the published results [20] with a 3-degree misalignment of the magnetic field. We note that our sample is also flux-grown. According to Ref. [20], the crystal growth method may influence the electron behavior of ZrTe₅ which is assumed to be critical for understanding the MR and MTP behavior at low temperatures. The samples used in both experiments also share similar Lifshitz transition temperatures, indicating that the reproduction of the identical magneto-thermoelectric behavior is reliable. According to Finite Element Method simulations with COMSOL Multiphysics using an a-axis thermal conductivity of $\kappa_a \sim 50 W/(m \cdot K)$ at 4 K, and beam width of $\sim 70 \mu m$, the temperature difference between two electrodes is found to be ~ 0.1 K. These results confirm that the photothermal method can faithfully extract the longitudinal MTP.

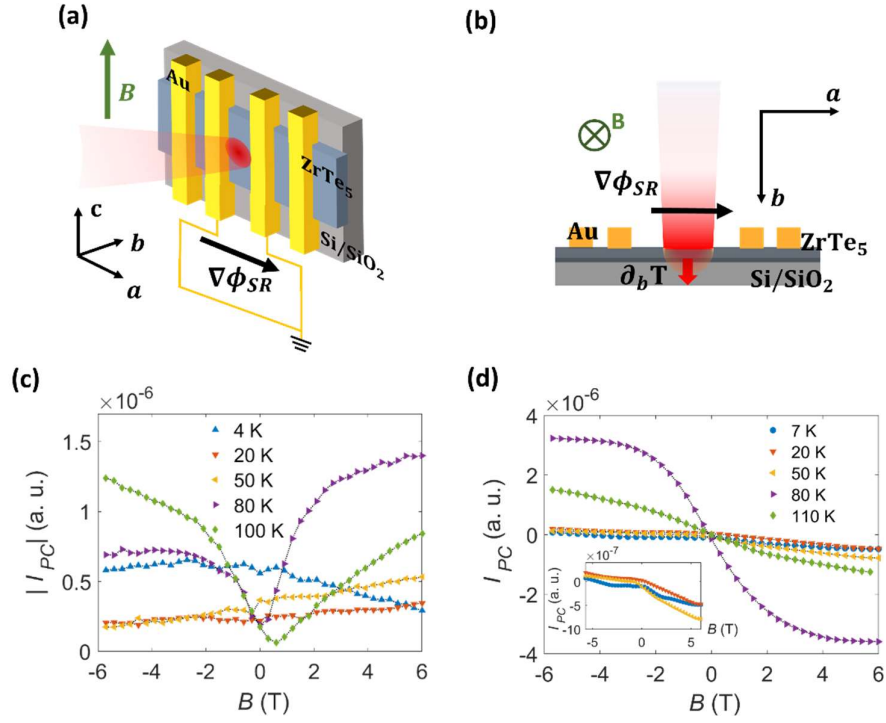


Fig. 3 Photothermal measurements with magnetic field perpendicular to a-axis of the crystal. (a) Experimental schematics with axes definition (b) Side-view of the schematics to characterize the direction of field B , thermal gradient ∇T and current $\nabla\phi_{SR}$. (c) In general cases, both signals, symmetric and anti-symmetric to magnetic field, contribute to the photocurrent measurement (d) By carefully aligning the laser spot to the center point between two contacts, the symmetric component can be removed, and the signal is solely contributed by the transverse component of the thermoelectric coefficient.

Next, we demonstrate the photothermal current results with the in-plane magnetic field aligned with c-axis to extract the magnetic field dependence of the Nernst coefficient (Fig. 3 (a)). Unlike in the previous measurement, we adjust the focusing spot of the laser to the middle point of two inner contacts. The laser generates thermal distributions in both in-plane and out-of-plane directions (Fig. 3(a) and side-view in 3(b)). In this configuration, because the magnetic field is aligned in-plane, the auxiliary field defined in the SR formalism still points straight from the drain to the source contact. Local current flowing in the c and b-axis direction doesn't contribute to the signal. The remaining contributing term is $j_{PC,a} \propto -S_{ba}\partial_b T + S_{aa}\partial_a T$. The S_{ba} contribution is anti-symmetric to the magnetic field whereas the S_{aa} contribution is symmetric. Without too much adjustment, we can readily observe the sum of both signals as shown in Fig. 3(c). We note that the in-plane (a-c plane) thermal gradient can generate in-plane photocurrent along both the +a and -a directions. Therefore, by carefully adjusting the position of the illumination spot, the

integration of the longitudinal contribution can be zero. In our simple sample configuration, we align the beam spot to the middle point between two contacts to make sure the S_{aa} contribution (symmetric in magnetic field) is always zero. The remaining S_{ba} component has 0 signal at $B=0$, as shown in Fig. 3(d). The contribution from S_{ba} depends on the thermal gradient along the out-of-plane ($\partial_b T$) direction as shown in Fig. 3(b). The sign of the gradient does not depend on where the photocurrent is generated. Therefore, the S_{ba} term is not canceled upon integration. As expected, our data in Fig. 3(d) shows the photothermal signal $I_{PC} \propto S_{ba}(B)$ is anti-symmetric in B (80K, 110K).

The saturating behavior of the transverse component of the MTP indicates an anomalous Nernst effect. The normal Drude-like Nernst coefficient $S_{ba}^N(B)$ decays to 0 at high field, while the anomalous Nernst coefficient $S_{ba}^A(B)$ saturates to a finite value. They can be approximated as

$$S_{ba}^N(B) = S_0^N \frac{\mu B}{1+(\mu B)^2}, \quad (3)$$

$$S_{ba}^A(B) = \Delta S_{ba}^A \tanh\left(\frac{B}{B_0}\right), \quad (4)$$

respectively [18,42]. Here, μ and B_0 are the charge mobility and the field where anomalous effect saturates. S_0^N and ΔS_{ba}^A denote the amplitudes of conventional and anomalous components of Nernst effect, respectively. At high field, we observe saturating Nernst effect rather than vanishing behavior at all temperature points investigated below 100 K, supporting the existence of anomalous thermoelectric effects [24]. Interestingly, at the base temperature of the experiment 7 K, we observe a weak quantum oscillation behavior arising from Landau bands. Compared with previous thermal transport results [24], the oscillation amplitude is weaker at similar temperatures, which is likely due to the heating effect of the 5 mW illumination on the sample surface.

IV. CONCLUSION

In this work, we investigated the magneto-thermoelectric power of 3D Dirac semimetal ZrTe₅. Instead of using canonical thermal transport techniques, we take advantage of the photothermal effect to induce local photocurrent density. Due to the simple geometry of the sample and contact configuration, we can selectively acquire the longitudinal and transverse components of the MTP. In the approximately parallel electric and magnetic field regime, our photothermal measurements reproduce nearly identical features to the result acquired in thermal transport measurement with an estimated 3-degree misalignment of the magnetic field [20]. In the transverse magnetic field regime, we measure the Nernst thermopower. The saturation behavior

at high magnetic fields is consistent with the anomalous Nernst effect previously observed in canonical thermal transport measurements. Our study highlights that photothermal experiment serves as a convenient and reliable method to study the thermoelectric behavior of bulk samples. This technique can also be broadly applied to thin films, thin crystals, and 2D materials.

Acknowledgments

This work at BNL was supported by the U.S. Department of Energy, Office of Basic Energy Sciences, Division of Materials Sciences and Engineering, under Contract No. DE-SC0012704. This research used resources of the Center for Functional Nanomaterials, which is a U.S. DOE Office of Science Facility, at Brookhaven National Laboratory. X.D. acknowledges support from the National Science Foundation (NSF) under award DMR-1808491. Nordita is supported in part by NordForsk. The authors acknowledge the valuable discussion with Dr. Bing Chen.

REFERENCE

- [1] Z. Wang, Y. Sun, X.Q. Chen, C. Franchini, G. Xu, H. Weng, X. Dai, Z. Fang, Dirac semimetal and topological phase transitions in A3Bi (A=Na, K, Rb), *Phys Rev B Condens Matter Mater Phys.* 85 (2012).
<https://doi.org/10.1103/PhysRevB.85.195320>.
- [2] S.M. Young, S. Zaheer, J.C.Y. Teo, C.L. Kane, E.J. Mele, A.M. Rappe, Dirac semimetal in three dimensions, *Phys Rev Lett.* 108 (2012).
<https://doi.org/10.1103/PhysRevLett.108.140405>.
- [3] X. Wan, A.M. Turner, A. Vishwanath, S.Y. Savrasov, Topological semimetal and Fermi-arc surface states in the electronic structure of pyrochlore iridates, *Phys Rev B Condens Matter Mater Phys.* 83 (2011).
<https://doi.org/10.1103/PhysRevB.83.205101>.
- [4] N.P. Armitage, E.J. Mele, A. Vishwanath, Weyl and Dirac semimetals in three-dimensional solids, *Rev Mod Phys.* 90 (2018).
<https://doi.org/10.1103/RevModPhys.90.015001>.
- [5] K. Fukushima, D.E. Kharzeev, H.J. Warringa, Chiral magnetic effect, *Physical Review D - Particles, Fields, Gravitation and Cosmology.* 78 (2008).
<https://doi.org/10.1103/PhysRevD.78.074033>.
- [6] D.E. Kharzeev, H.J. Warringa, Chiral magnetic conductivity, *Physical Review D - Particles, Fields, Gravitation and Cosmology.* 80 (2009).
<https://doi.org/10.1103/PhysRevD.80.034028>.
- [7] D.E. Kharzeev, The Chiral Magnetic Effect and anomaly-induced transport, *Prog Part Nucl Phys.* 75 (2014) 133–151. <https://doi.org/10.1016/j.pnpnp.2014.01.002>.
- [8] S. Kaushik, D.E. Kharzeev, E.J. Philip, Chiral magnetic photocurrent in Dirac and Weyl materials, *Phys Rev B.* 99 (2019).
<https://doi.org/10.1103/PhysRevB.99.075150>.
- [9] D.E. Kharzeev, Topologically induced local P and CP violation in QCD x QED, (2009). <https://doi.org/10.1016/j.aop.2009.11.002>.
- [10] Q. Li, D.E. Kharzeev, C. Zhang, Y. Huang, I. Pletikosić, A. V. Fedorov, R.D. Zhong, J.A. Schneeloch, G.D. Gu, T. Valla, Chiral magnetic effect in ZrTe5, *Nat Phys.* 12 (2016) 550–554. <https://doi.org/10.1038/nphys3648>.
- [11] J. Xiong, S.K. Kushwaha, T. Liang, J.W. Krizan, M. Hirschberger, W. Wang, R.J. Cava, N.P. Ong, Evidence for the chiral anomaly in the Dirac semimetal Na3Bi, *Science* (1979). 350 (2015) 413–416. <https://doi.org/10.1126/science.aac6089>.
- [12] C.Z. Li, L.X. Wang, H. Liu, J. Wang, Z.M. Liao, D.P. Yu, Giant negative magnetoresistance induced by the chiral anomaly in individual Cd3As2 nanowires,

- Nat Commun. 6 (2015). <https://doi.org/10.1038/ncomms10137>.
- [13] H. Li, H. He, H.Z. Lu, H. Zhang, H. Liu, R. Ma, Z. Fan, S.Q. Shen, J. Wang, Negative magnetoresistance in Dirac semimetal Cd₃As₂, Nat Commun. 7 (2016). <https://doi.org/10.1038/ncomms10301>.
- [14] X. Huang, L. Zhao, Y. Long, P. Wang, D. Chen, Z. Yang, H. Liang, M. Xue, H. Weng, Z. Fang, X. Dai, G. Chen, Observation of the chiral-anomaly-induced negative magnetoresistance: In 3D Weyl semimetal TaAs, Phys Rev X. 5 (2015). <https://doi.org/10.1103/PhysRevX.5.031023>.
- [15] Y. Li, Z. Wang, P. Li, X. Yang, Z. Shen, F. Sheng, X. Li, Y. Lu, Y. Zheng, Z.A. Xu, Negative magnetoresistance in Weyl semimetals NbAs and NbP: Intrinsic chiral anomaly and extrinsic effects, Front Phys (Beijing). 12 (2017). <https://doi.org/10.1007/s11467-016-0636-8>.
- [16] F. Arnold, C. Shekhar, S.C. Wu, Y. Sun, R.D. Dos Reis, N. Kumar, M. Naumann, M.O. Ajeesh, M. Schmidt, A.G. Grushin, J.H. Bardarson, M. Baenitz, D. Sokolov, H. Borrmann, M. Nicklas, C. Felser, E. Hassinger, B. Yan, Negative magnetoresistance without well-defined chirality in the Weyl semimetal TaP, Nat Commun. 7 (2016). <https://doi.org/10.1038/ncomms11615>.
- [17] J.M. Ziman, Electrons and phonons: the theory of transport phenomena in solids, Oxford university press, 2001.
- [18] T. Liang, Q. Gibson, J. Xiong, M. Hirschberger, S.P. Koduvayur, R.J. Cava, N.P. Ong, Evidence for massive bulk dirac fermions in Pb_{1-x}Sn_xSe from nernst and thermopower experiments, Nat Commun. 4 (2013). <https://doi.org/10.1038/ncomms3696>.
- [19] Z. Jia, C. Li, X. Li, J. Shi, Z. Liao, D. Yu, X. Wu, Thermoelectric signature of the chiral anomaly in Cd₃As₂, Nat Commun. 7 (2016). <https://doi.org/10.1038/ncomms13013>.
- [20] Y. Li, H. Wang, J. Wang, C. Wang, Y. Liu, J. Ge, J. Niu, W. Zhang, P. Wang, R. Bi, J. Zhang, J.Y. Dai, J. Yan, D. Mandrus, N. Samarth, H. Lu, X. Wu, J. Wang, Anomalous magnetothermoelectric behavior in massive Dirac materials, Phys Rev B. 107 (2023). <https://doi.org/10.1103/PhysRevB.107.085140>.
- [21] H. Chi, C. Zhang, G. Gu, D.E. Kharzeev, X. Dai, Q. Li, Lifshitz transition mediated electronic transport anomaly in bulk ZrTe₅, New J Phys. 19 (2017). <https://doi.org/10.1088/1367-2630/aa55a3>.
- [22] W. Zhang, P. Wang, G. Gu, X. Wu, L. Zhang, Negative longitudinal magnetothermopower in the topological semimetal ZrTe₅, Phys Rev B. 102 (2020). <https://doi.org/10.1103/PhysRevB.102.115147>.

- [23] P.M. Lozano, G. Cardoso, N. Aryal, D. Nevola, G. Gu, A. Tsvetik, W. Yin, Q. Li, Anomalous Hall effect at the Lifshitz transition in ZrTe₅, *Phys Rev B*. 106 (2022). <https://doi.org/10.1103/PhysRevB.106.L081124>.
- [24] J.L. Zhang, C.M. Wang, C.Y. Guo, X.D. Zhu, Y. Zhang, J.Y. Yang, Y.Q. Wang, Z. Qu, L. Pi, H.Z. Lu, M.L. Tian, Anomalous Thermoelectric Effects of ZrTe₅ in and beyond the Quantum Limit, *Phys Rev Lett*. 123 (2019). <https://doi.org/10.1103/PhysRevLett.123.196602>.
- [25] Y. Liu, H. Pi, K. Watanabe, T. Taniguchi, G. Gu, Q. Li, H. Weng, Q. Wu, Y. Li, Y. Xu, Gate-Tunable Multiband Transport in ZrTe₅ Thin Devices, *Nano Lett*. 23 (2023) 5334–5341. <https://doi.org/10.1021/acs.nanolett.3c01528>.
- [26] S. Galeski, T. Ehmcke, R. Wawrzyńczak, P.M. Lozano, K. Cho, A. Sharma, S. Das, F. Küster, P. Sessi, M. Brando, R. Kuchler, A. Markou, M. König, P. Swekis, C. Felser, Y. Sassa, Q. Li, G. Gu, M. V Zimmermann, O. Ivashko, D.I. Gorbunov, S. Zherlitsyn, T. Förster, S.S.P. Parkin, J. Wosnitza, T. Meng, J. Gooth, Origin of the quasi-quantized Hall effect in ZrTe₅, *Nat Commun*. 12 (2021) 3197. <https://doi.org/10.1038/s41467-021-23435-y>.
- [27] F. Tang, P. Wang, M. He, M. Isobe, G. Gu, Q. Li, L. Zhang, J.H. Smet, Two-Dimensional Quantum Hall Effect and Zero Energy State in Few-Layer ZrTe₅, *Nano Lett*. 21 (2021) 5998–6004. <https://doi.org/10.1021/acs.nanolett.1c00958>.
- [28] A. Gourgout, M. Leroux, J.-L. Smir, M. Massoudzadegan, R.P.S.M. Lobo, D. Vignolles, C. Proust, H. Berger, Q. Li, G. Gu, C.C. Homes, A. Akrap, B. Fauqué, Magnetic freeze-out and anomalous Hall effect in ZrTe₅, *NPJ Quantum Mater*. 7 (2022) 71. <https://doi.org/10.1038/s41535-022-00478-y>.
- [29] S. Galeski, H.F. Legg, R. Wawrzyńczak, T. Förster, S. Zherlitsyn, D. Gorbunov, M. Uhlarz, P.M. Lozano, Q. Li, G.D. Gu, C. Felser, J. Wosnitza, T. Meng, J. Gooth, Signatures of a magnetic-field-induced Lifshitz transition in the ultra-quantum limit of the topological semimetal ZrTe₅, *Nat Commun*. 13 (2022) 7418. <https://doi.org/10.1038/s41467-022-35106-7>.
- [30] W. Shockley, Currents to conductors induced by a moving point charge, *J Appl Phys*. 9 (1938) 635–636. <https://doi.org/10.1063/1.1710367>.
- [31] J.C.W. Song, L.S. Levitov, Shockley-Ramo theorem and long-range photocurrent response in gapless materials, *Phys Rev B Condens Matter Mater Phys*. 90 (2014). <https://doi.org/10.1103/PhysRevB.90.075415>.
- [32] Q. Ma, C.H. Lui, J.C.W. Song, Y. Lin, J.F. Kong, Y. Cao, T.H. Dinh, N.L. Nair, W. Fang, K. Watanabe, T. Taniguchi, S.-Y. Xu, J. Kong, T. Palacios, N. Gedik, N.M. Gabor, P. Jarillo-Herrero, Giant intrinsic photoresponse in pristine graphene, *Nat*

- Nanotechnol. 14 (2019) 145–150. <https://doi.org/10.1038/s41565-018-0323-8>.
- [33] Y. Shao, R. Jing, S.H. Chae, C. Wang, Z. Sun, E. Emmanouilidou, S. Xu, D. Halbertal, B. Li, A. Rajendran, F.L. Ruta, L. Xiong, Y. Dong, A.S. McLeod, S.S. Sunku, J.C. Hone, J. Moore, J. Orenstein, J.G. Analytis, A.J. Millis, N. Ni, D. Xiao, D.N. Basov, Nonlinear nanoelectrodynamics of a Weyl metal, *Proceedings of the National Academy of Sciences*. 118 (2021) e2116366118. <https://doi.org/10.1073/pnas.2116366118>.
- [34] H. Cao, G. Aivazian, Z. Fei, J. Ross, D.H. Cobden, X. Xu, Photo-Nernst current in graphene, *Nat Phys*. 12 (2016) 236–239. <https://doi.org/10.1038/nphys3549>.
- [35] Q. Ma, R. Krishna Kumar, S.-Y. Xu, F.H.L. Koppens, J.C.W. Song, Photocurrent as a multiphysics diagnostic of quantum materials, *Nature Reviews Physics*. 5 (2023) 170–184. <https://doi.org/10.1038/s42254-022-00551-2>.
- [36] Y. Zhang, C. Wang, L. Yu, G. Liu, A. Liang, J. Huang, S. Nie, X. Sun, Y. Zhang, B. Shen, J. Liu, H. Weng, L. Zhao, G. Chen, X. Jia, C. Hu, Y. Ding, W. Zhao, Q. Gao, C. Li, S. He, Z. Zhao, F. Zhang, S. Zhang, F. Yang, Z. Wang, Q. Peng, X. Dai, Z. Fang, Z. Xu, C. Chen, X.J. Zhou, Electronic evidence of temperature-induced Lifshitz transition and topological nature in ZrTe₅, *Nat Commun*. 8 (2017). <https://doi.org/10.1038/ncomms15512>.
- [37] Y. Tian, N. Ghassemi, J.H. Ross, Dirac electron behavior and NMR evidence for topological band inversion in ZrTe₅, *Phys Rev B*. 100 (2019). <https://doi.org/10.1103/PhysRevB.100.165149>.
- [38] O. Shigeto, S. Takashi, I. Masayuki, Giant Resistivity Anomaly in ZrTe₅, *J Physical Soc Japan*. 49 (1980) 839–840. <https://doi.org/10.1143/JPSJ.49.839>.
- [39] W. Knap, C. Skierbiszewski, A. Zduniak, E. Litwin-Staszewska, D. Bertho, F. Kobbi, J.L. Robert, G.E. Pikus, F.G. Pikus, S. V Iordanskii, V. Mosser, K. Zekentes, Y.B. Lyanda-Geller, Weak antilocalization and spin precession in quantum wells, 1996.
- [40] H.Z. Lu, S.Q. Shen, Weak antilocalization and localization in disordered and interacting Weyl semimetals, *Phys Rev B Condens Matter Mater Phys*. 92 (2015). <https://doi.org/10.1103/PhysRevB.92.035203>.
- [41] B. Zhao, P. Cheng, H. Pan, S. Zhang, B. Wang, G. Wang, F. Xiu, F. Song, Weak antilocalization in Cd₃As₂ thin films, *Sci Rep*. 6 (2016). <https://doi.org/10.1038/srep22377>.
- [42] T. Liang, J. Lin, Q. Gibson, T. Gao, M. Hirschberger, M. Liu, R.J. Cava, N.P. Ong, Anomalous Nernst Effect in the Dirac Semimetal Cd₃As₂, *Phys Rev Lett*. 118 (2017). <https://doi.org/10.1103/PhysRevLett.118.136601>.

